

A Direct Theory of Viscous Fluid Flow in Pipes II. Flow of Incompressible Viscous Fluid in Curved Pipes

A. E. Green, P. M. Naghdi and M. J. Stallard

Phil. Trans. R. Soc. Lond. A 1993 **342**, 543-572
doi: 10.1098/rsta.1993.0032

Email alerting service

Receive free email alerts when new articles cite this article - sign up in the box at the top right-hand corner of the article or click [here](#)

To subscribe to *Phil. Trans. R. Soc. Lond. A* go to:
<http://rsta.royalsocietypublishing.org/subscriptions>

A direct theory of viscous fluid flow in pipes

II. Flow of incompressible viscous fluid in curved pipes

BY A. E. GREEN¹, P. M. NAGHDI² AND M. J. STALLARD²

¹*Mathematical Institute, University of Oxford, 24–29 St. Giles',
Oxford OX1 3LB, U.K.*

²*Department of Mechanical Engineering, University of California, Berkeley,
California 94720, U.S.A.*

Contents

	PAGE
1. Preliminary remarks	544
(a) A brief history of the problem	544
(b) The nature of the analytical solution obtained	549
(c) Scope of the paper	550
2. Formulation of the problem	551
3. Choice of the weighting functions associated with an hierarchical structure of the theory	556
4. Reduction of the equations of motion of the direct theory	558
5. Complete solution for circular pipes of circular cross section	561
(a) The procedure for obtaining a complete solution	562
(b) Treatment of singular points of the solution	562
(c) A procedure for calculation of the streamlines and axial velocity contours	563
(d) Results of the calculations for circular pipes of circular cross section	563
(e) Further remarks on the detailed nature of the flow	567
Appendix A	570
References	571

This paper is a companion to Part I under the same title and is concerned with the development of an analytical solution (via a *direct* formulation) for flow of an incompressible viscous fluid in curved pipes. Although a major portion of the analysis is presented for circular pipes of elliptical cross section, detailed calculations are carried out only for pipes of circular cross section. These calculations include the friction loss factor and the velocity contours, both of which are presented over a range of Dean number that significantly goes beyond the corresponding range of recent numerical solutions and the available experimental data. The results obtained show very favourable agreements with existing experimental data and several recent numerical solutions of the same problem based on the Navier–Stokes equations. Also included (for pipes of circular cross section) is a comparison of the multiple solutions and bifurcation points, as predicted by the present analytical solution, with

Phil. Trans. R. Soc. Lond. A (1993) **342**, 543–572

© 1993 The Royal Society

Printed in Great Britain

543

corresponding available information from several recent numerical solutions of the problem.

1. Preliminary remarks

This paper complements a previous one by Green & Naghdi (1990) under the same title (hereafter referred to as Part I), which contains the basic development of a direct general theory of viscous fluid flow in pipes or tubes. The main purpose of the present paper is to obtain, with the use of the basic equations of Part I, an analytical solution for flow of an incompressible viscous fluid in curved pipes. Although a major portion of the analysis (including the final algebraic system of equations in §4) is presented for circular pipes of elliptical cross section (figure 1), detailed calculations are carried out only for pipes of circular cross section along with extensive comparisons of our calculated results with existing experimental data and several recent solutions of the same problem obtained numerically from the Navier–Stokes equations.

For general background information on the subject, reference may be made to two books (Pedley 1980; Ward-Smith 1980), each of which includes a chapter on flow in curved pipes. Also, a detailed survey of flow in curved pipes has been given by Berger *et al.* (1983), and an additional source of references is a recent review paper by Itō (1987), who covers a wider range of topics but with less analysis.

To make the contents of this paper accessible to a fairly wide range of readers, who may neither be aware of the existing difficulties in the general problem of flow in curved pipes nor of the nature of the direct theories of the type utilized, in the remainder of this section we describe in separate subsections various aspects of the subject, including a rapid summary of the history of the problem, the available experimental data for circular pipes of circular cross section and the more recent literature on the numerical solution of the problem obtained with the use of the Navier–Stokes equations, the nature of the analytical solution obtained, as well as the scope of the paper.

(a) *A brief history of the problem*

For definiteness and with reference to the special case of figure 1 when $a = b$, consider the flow of an incompressible linear viscous fluid in a curved pipe (or tube) of circular cross section of radius b whose centre-line forms a circle of radius R . The ratio

$$\delta = b/R \quad (1.1)$$

is frequently used as a measure of the curvature of the pipe and is called the curvature ratio. It should be noted here that the definition (1.1) and other definitions in this section are valid also in the case of pipes of elliptical cross section and that it is not necessary at this time (or even in the developments of §§2–4) to distinguish between the major and minor axes.

We are interested here in flows which are laminar, steady and fully developed and accordingly are parametrized by a non-dimensional flow quantity such as the Reynolds number Re based on an average streamwise velocity, say w (such as the component of the average velocity along the centre-line of the pipe) defined by

$$Re = 2bw/\nu, \quad (1.2)$$

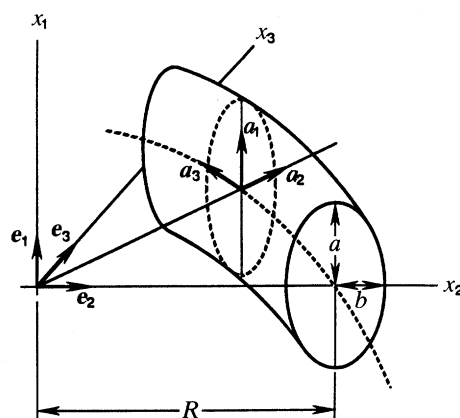


Figure 1. A segment of the curved elliptical pipe showing its centre-line (dashed curve) which forms a circle of radius R . The elliptical cross section of the pipe in the x_1 - x_2 plane of the rectangular Cartesian coordinate system has the semi-axes a and b . Also shown are the orthonormal bases \mathbf{e}_i and \mathbf{a}_i .

where ν is the kinematic viscosity, i.e. the ratio of the shear viscosity to the mass density of the fluid. However, for the problem of the flow in curved pipes, it is more convenient to use instead the Dean number κ defined by

$$\kappa = Re \delta^{\frac{1}{2}}. \quad (1.3)$$

(There are a variety of definitions of Dean number, depending on what value one uses for the velocity w . These definitions and their relation to (1.3) are discussed by Berger *et al.* (1983).)

An important feature of the flow in a curved pipe is the friction factor λ_c defined to be the inverse of the mean speed w times the cross-sectional area A of the pipe, i.e.

$$\lambda_c = 1/Aw = 1/Q_c, \quad (1.4)$$

where Q_c denotes the volume flow rate. The friction loss ratio f is defined as the ratio of the friction factor in the curved pipe to the corresponding friction factor λ_s in a straight pipe of the same cross section and for the same pressure gradient. By virtue of (1.4), the friction loss ratio can also be expressed as the ratio of the volume flow rate Q_s in a straight pipe of the same cross section to the corresponding flow rate Q_c in the curved pipe for the same pressure gradient, i.e.

$$f = \lambda_c/\lambda_s = Q_s/Q_c. \quad (1.5)$$

Among other relevant quantities of interest is, of course, the detailed nature of the velocity field.

The first study of the subject of curved pipe flow is due to Dean (1927, 1928), who analysed the problem with the use of a perturbation procedure from straight pipe flow for infinitesimally small curvature ratio and small Dean number. For clarity we observe that since the flow depends on the two parameters (1.1) and (1.3), basically speaking, two distinct perturbation schemes should be used, one in δ and another in κ . In this connection, however, it should be noted that Dean (1927, 1928) did not carry out the perturbation for small δ (and actually set $\delta = 0$) but carried out his perturbation in such a manner that the effect of curvature was accounted for by the introduction of the factor $\delta^{\frac{1}{2}}$ in the definition of the Dean number (1.3). Moreover,

with the use of the exact equations of the three-dimensional theory (the Navier–Stokes equations) by linearizing near the solution for a straight pipe (Poiseuille flow), he obtained a two-term series expansion in κ^2 for the flow in a curved pipe. This solution, which indicates the presence of a cross-flow consisting of two counter-rotating vortices in the cross section, represents the first explicit calculation for friction loss indicating the effect of curvature on the flow in the pipe.

The ideas of Dean were later extended by Topakoglu (1967), who obtained a double perturbation series expansion in κ^2 and δ for the flow to second order. His results include also the low order geometric effects of curvature, as well as the kinetical effects (due to cross-flow). The series solution of Topakoglu (1967) was subsequently carried out to seventh order by Larrain & Bonilla (1970), although the significance of such a development is questionable.

More recently, Van Dyke (1978) reconsidered Dean's (1928) series solution, carried out the perturbations to the 12th order in κ^2 , and then by a suitable transformation he generated an extended Stokes series which he claimed to be appropriate for all values of Dean number. He then ascertained that as Dean number becomes large, the friction loss has the asymptotic behaviour

$$f \sim \kappa^{\frac{1}{2}} \quad \text{as } \kappa \rightarrow \infty. \quad (1.6)$$

Another avenue of approach to the study of this problem was initiated by Adler (1934), who made use of a boundary layer analysis. In Adler's analysis, the flow at a cross section of the pipe is assumed to consist of a boundary layer near the pipe wall and a core regarded to be unaffected by viscous effects (and thus treated as an inviscid fluid). Such an assumption is reasonable only for large κ and correspondingly yields asymptotic estimates for friction loss of the form

$$f \sim \kappa^{\frac{1}{2}} \quad \text{as } \kappa \rightarrow \infty. \quad (1.7)$$

Similar analyses using the boundary layer approach and different methods of solution have been carried out by Barua (1963) and Itō (1969) and both of these yield solutions of the form (1.7).

The problem has also been studied numerically by using the exact three-dimensional equations. Early studies have been improved upon considerably in recent years and because of this it will suffice to only cite the most recent of these papers. Most commonly, the Navier–Stokes equations are discretized by finite differences and solved by using Newton's method. Other discretizations using finite element methods, spectral methods or combinations of these methods have also been employed. Difficulties are encountered in solving the resulting nonlinear equations for large Dean number because of the slowness of convergence and numerical 'instability' common for high Reynolds number flow. This problem may be avoided to some degree by the use of the so-called 'upwind' difference schemes (Collins & Dennis 1975) or transformation to diagonal dominant systems (Dennis 1980) when using finite differences or by use of Euler–Newton continuation techniques (Winters & Brindley 1984; Yang & Keller 1986). The largest value of Dean number for which results have been reported is $\kappa = 1290$ ($\log \kappa \sim 3.1$) by Soh & Berger (1987). Solutions by Collins & Dennis (1975) up to moderate values of Dean number ($\kappa \sim 360$ or $\log \kappa \sim 2.6$) indicate a basic flow much like the two-vortex cross flow of the Dean (1928) solution. These solutions showed agreement with (1.7) in contradiction with the analysis of Van Dyke (1978) who argued that the discrepancy was due to the inaccuracies in the calculations of Collins & Dennis. To address this claim, Dennis

(1980) obtained accurate numerical solutions and quantitative error estimates which supported the earlier conclusions of Collins & Dennis (1975).

The most interesting feature of the recent numerical solutions is the prediction of the existence of multiple solutions of the Navier–Stokes equations for Dean number $\kappa > 110$ ($\log \kappa > 2.0$). A second set of solutions characterized by four vortices in a cross section, which was first discovered by Dennis & Ng (1982), has been confirmed by the more recent computations of Winters & Brindley (1984) and Yang & Keller (1986); these latter authors go on to discover another set characterized by six vortices. Daskopoulos & Lenhoff (1989) also reported a third set of solutions, but it appears to be different (with four vortices) than that of Yang & Keller (with six vortices); in this connection, compare figs 7 and 8 of Yang & Keller (1986) with figs 6 and 7 of Daskopoulos & Lenhoff (1989). The detailed nature of the velocity field differs significantly between these sets of solutions (those with two, four and six vortices calculated by Dennis & Ng, Winters & Brindley, Yang & Keller and Daskopoulos & Lenhoff). (To demonstrate this difference in the velocity, Daskopoulos & Lenhoff (1989) plot the magnitude of the cross-flow velocity at a particular location in the cross section versus the Dean number and display in their fig. 9 marked differences between their own three sets of solutions.) But the friction loss is nearly the same for all three sets and, at least in the range that the friction loss has been calculated, fits the relation (1.7) indicating additional support for this latter expression.

For the purpose of later comparison, figure 2*a,b* shows a converted log–log plot of the numerical results of Yang & Keller (1986, figs 2 and 3) in terms of the definition of Dean number used here along with a well-known set of experimental data which we describe in the next paragraph. The graphical presentations in figure 2 correspond to numerical results obtained by Yang & Keller for different measures of ‘finess’ of discretization in their numerical procedure. Figure 2*b* corresponds to a finer discretization than that of figure 2*a*; see §5 of Yang & Keller (1986). Also displayed in figure 2 by a dashed line is the result of Van Dyke’s (1978) prediction for the friction loss.

Experiments on flow in curved pipes of circular cross section have been carried out since the early part of the 20th century (Eustice 1910). Detailed measurements of friction loss and some measurements of the velocity field at various Dean numbers in the range $4 < \kappa < 4000$ have been made by White (1929), Taylor (1929), Adler (1934), Keulegan & Beij (1937) and Itō (1959). (Some additional experimental results have been reported recently by Ramshankar & Sreenivasan (1988), but we postpone further comments on their work until the last paragraph of this subsection.) Many of these results have been compiled by Itō (1959) in a well-known graph of the logarithm of friction loss versus the logarithm of Dean number. It is evident from this graph that there is an envelope or lower bound to friction loss which has been fitted by various authors over different ranges of Dean number, the most recent being that of Hasson (1955) over a wide range of Dean number ($\kappa < 5000$ or $\log \kappa < 3.7$) and of the form

$$f = A\kappa^{\frac{1}{2}} + B \quad (1.8)$$

with $A = 0.0969$ and $B = 0.556$. In connection with the multiple solutions discovered recently in the numerical solutions (Dennis & Ng 1982; Yang & Keller 1986) it is perhaps interesting to note that the four-vortex solution has been observed experimentally (Cheng *et al.* 1983) but no measurements of friction loss have been reported for it.

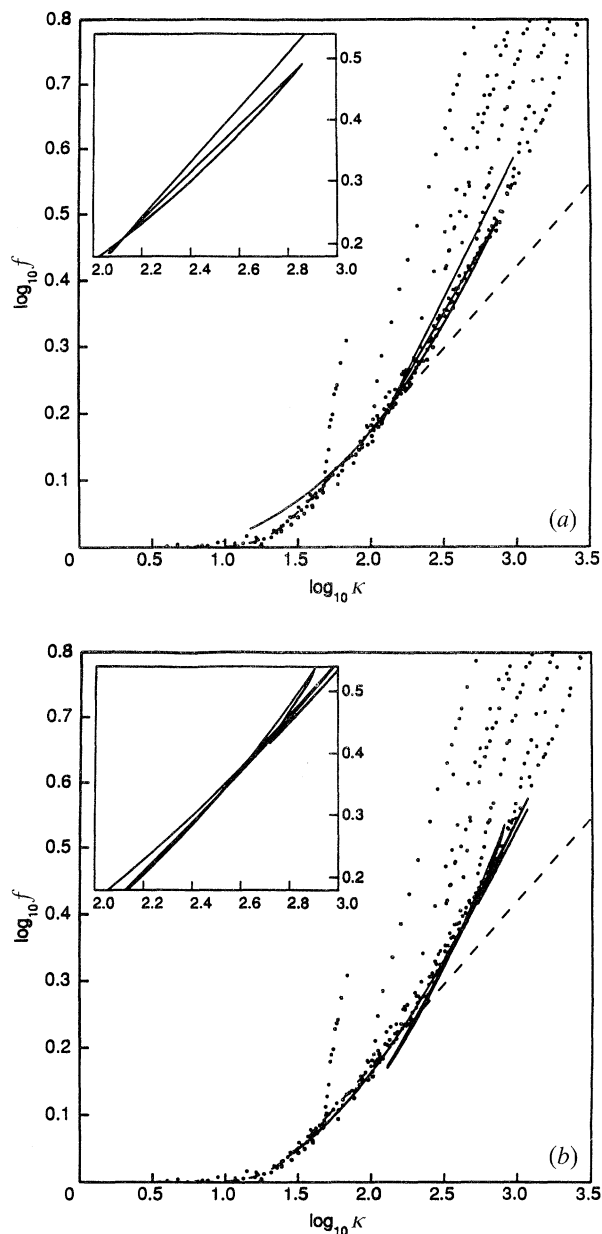


Figure 2. Plots of numerical results of Yang & Keller (1986) corresponding to very small curvature ratio ($\delta = 0$) for the friction loss over an intermediate range of the Dean number. Parts (a) and (b) are converted versions of Yang & Keller's figs 2 and 3, respectively, in terms of the more common definition of the Dean number given by equation (1.3). Also exhibited in these figures are the experimental data from Itō (1959) collectively designated by dots and the prediction of Van Dyke (1978) by the dashed line.

The discrepancy between the experimental envelope and the theoretical predictions of Van Dyke (1978) for friction loss has been of some concern over the years (Dennis 1980). This issue has been reconsidered in a recent paper of Ramshankar &

Sreenivasan (1988), who conducted some new experiments in the range of $200 < \kappa < 2000$ ($2.3 < \log \kappa < 3.3$), which in some sense was intended to support Van Dyke's result. Their data in this range lie between the previous experimental measurements and the result of Van Dyke. These authors (Ramshankar & Sreenivasan 1988) argue that their data are more relevant to the problem under discussion, but they also acknowledge the numerical solution of Dennis & Ng (1982) which is based on the full Navier–Stokes equations (see Ramshankar & Sreenivasan 1988, last paragraph). However, in view of the additional numerical solutions of the problem by Yang & Keller, Daskopoulos & Lenhoff and Soh & Berger (cited in the paragraph before last), it seems rather futile to give credence to asymptotic solutions of the type used by Van Dyke (1978) as has been pointed out previously by Yang & Keller (1986, second paragraph of §1 and last paragraph of §5 of their paper).

(b) *The nature of the analytical solution obtained*

The eulerian formulation of the direct theory of Part I (Green & Naghdi 1993) when applied to the problem of flow of an incompressible newtonian viscous fluid in curved pipes yields a system of partial differential equations for the velocity and the director velocities. The independent variables in these equations are a coordinate ζ along a curve (such as the centre-line of the pipe) and time t . Derivatives with respect to t of the first order and with respect to ζ of the second order of the velocities occur in this system of equations, which symbolically may be represented by a system of vector equations of the form

$$F(w_{Ni}, w_{Ni,\zeta}, w_{Ni,\zeta\zeta}, w_{Ni,t}; A, B) = \mathbf{0}. \quad (1.9)$$

In (1.9), a comma following the subscript N denotes partial differentiation, $w_{Ni} = (v_i, w_{1i}, w_{2i}, \dots)$ stand for the components of the velocity \mathbf{v} and the director velocities of the Cosserat curve (see (2.3) and (2.5) of Part I), the symbol A represents a set of variables arising from the nature of the geometry and other three-dimensional characteristics of the flow, such as the minor and major axes of the elliptical cross section, radius of the curvature of the centre-line of the curved pipe or viscosity, and B represents a set of auxiliary variables arising as a consequence of the constraints (such as incompressibility) imposed on the kinematical variables in the theory. The sets of quantities A and B , as well as the functional dependence of F on the set A , involve a number of constitutive coefficients occurring in the theory. Although the choice of these coefficients is restricted by the consequence of balance of moment of momentum (eq. (2.15) in Part I), it is possible that some members of the set A may depend on ζ and t as, for example, in the case of curved or straight pipes of varying cross section. Since the constitutive coefficients in the three-dimensional theory associated with an incompressible linear viscous fluid are constants, their effect in the set A does not contribute to this dependence on ζ and t ; it is only the shape factors which may be dependent on time and coordinates.

Under the conditions of steady and fully developed flow, i.e. $w_{Ni,t} = 0$ and $w_{Ni,\zeta} = 0$, a more simplified system of equations will result from (1.9) in the form

$$F(w_{Ni}, \mathbf{0}, \mathbf{0}, \mathbf{0}; A, B) = G(w_{Ni}; A, B) = \mathbf{0}. \quad (1.10)$$

It is of interest to contrast the purely algebraic (nonlinear) system of equations (1.10) with that of a corresponding system of equations in the exact three-dimensional theory. With the notation v_i^* (in a convenient coordinate system) for the components

of the velocity vector in the three-dimensional theory, the Navier–Stokes equations when specialized to steady, fully developed flow of an incompressible viscous fluid in curved or straight pipes take the form

$$H^*(v_i^*, v_{i,\alpha}^*, v_{i,\alpha\alpha}^*; A^*, B^*) = \mathbf{0}, \quad (1.11)$$

where the subscript α takes the values 1, 2, $(\cdot)_{,\alpha}$ denotes partial differentiation with respect to coordinates ζ^α (of the three-dimensional coordinate system $\zeta^i = (\zeta^\alpha, \zeta)$) and A^*, B^* represent quantities analogous to A, B .

(c) *Scope of the paper*

With the use of the basic theory in §2 of Part I, the problem of flow of an incompressible viscous fluid in a circular pipe of an elliptical cross section is formulated in §2. The developments in §2 include consideration of several restrictions imposed on the kinematical ingredients $(\mathbf{v}, \mathbf{w}_N^i)$, which arise from appropriate constraints (such as the incompressibility condition) and their consequent effects on various kinetical variables in the basic differential equations of the general theory (§2 of Part I). These constraints result in a significant simplification of the basic theory and lead to a system of two scalar nonlinear partial differential equations (see (2.26)), which takes into account the symmetry in the cross-flow directions.

Eventually the system of equations just referred to, after the use of appropriate constitutive equations, the specification of the pressure gradient (in conformity with the type of flow in curved pipe under discussion) and the boundary and other flow conditions, determine the desired velocity fields $(\mathbf{v}, \mathbf{w}_N^i)$. It is important to note here that this manner of determination of the velocity fields in the direct theory also requires the knowledge of the weighting functions λ_N^i . The selection of such weighting functions represents an important aspect of the formulation of the problem: they occur in expressions such as (A 28)–(A 31) in Appendix A of Part I; and it is from these expressions that the constitutive equations in the direct theory are calculated in harmony with the usual stress constitutive equation for an incompressible newtonian viscous fluid of the three-dimensional theory.

The next two sections of the paper deal, respectively, with the choice of the weighting functions and a reduction of the equations of motion in a suitable non-dimensional form. With the help of certain observations pertaining to cross-flow symmetry, the structure of the incompressibility condition in terms of the curvilinear coordinates utilized, and the no-slip condition at the pipe wall, suitable weighting functions are chosen. Closed form analytical expressions of the constitutive results involving the weighting functions, the curvature ratio δ and the aspect ratio $\epsilon = b/a$ of the elliptical cross section of the pipe are then derived (see also figure 1). The final form of the five relevant constitutive coefficients which occur in the non-dimensional constitutive equations are recorded in Appendix A, where the details of the calculations are also illustrated in one representative case. Next, after substitution of these results in the constrained equations of motion obtained in §2, we obtain in §4 the final non-dimensional equations of motion in the forms (4.8) and (4.9) for circular pipes of elliptical cross section.

Detailed calculations based on the equations of motion for circular pipes of circular cross section derived in §4 results depicted in five figures, along with extensive comparisons with existing experimental data and recent numerical calculations from the Navier–Stokes equations are discussed in §5. The results in figure 5 are in very

good agreement with the corresponding numerical solutions of the Navier–Stokes equations (Yang & Keller 1986, and others), as well as with Hasson's (1955) envelope for the experimental data. (Although the results are reported over the range $0 \leq \log \kappa \leq 3.5$, the calculations were actually carried out up to $\log \kappa = 4$, which is well beyond previously obtained numerical solutions based on the Navier–Stokes equations.) The results of the calculations from the direct theory also exhibit multiple solutions, which can be seen by the 'loops' in the friction loss curve shown in figure 5. These multiple solutions are intimately related to the vortical structure of the flow in the cross section of the pipe, as discussed in §§5*d* and 5*e*, and are compared with the corresponding numerical calculations of Yang & Keller (1986) and Daskopoulos & Lenhoff (1989).

Before closing this subsection, it should be mentioned that most of the algebraic calculations were carried out with the help of the computer program VAXIMA. This is a symbolic manipulation program which is based on the program MACSYMA available from Mathlab Group, Laboratory for Computer Science, MIT.

2. Formulation of the problem

We apply in this section the basic theory of Part I to the steady, fully developed, flow of an incompressible viscous fluid in a curved pipe of uniform elliptical cross section. Recalling the notation x_i and \mathbf{e}_i associated with a fixed system of a rectangular cartesian coordinate system introduced in (Part I, §3), a curved pipe of elliptical cross section with semi-axis a and b in the x_1 – x_2 plane and with centre at $x_2 = R$ (see figure 1) can be described as a surface of revolution formed by rotating the elliptical section about the x_1 -axis. The centre-line of the pipe then forms a circle of radius R in the x_2 – x_3 plane with its centre at the origin of the rectangular cartesian coordinate system.

Preliminary to the development that follows we introduce a set of orthogonal curvilinear coordinates $\zeta^i = (\zeta^1, \zeta^2, \zeta^3)$ ($i = 1, 2, 3$), by the transformation (see also figure 1)

$$x_1 = \zeta^1, \quad x_2 = (R + \zeta^2) \cos \zeta^3/R, \quad x_3 = (R + \zeta^2) \sin \zeta^3/R \quad (2.1)$$

$$\text{and its inverse} \quad \zeta^1 = x_1, \quad \zeta^2 = (x_2^2 + x_3^2)^{1/2} - R, \quad \zeta^3 = R \arctan(x_3/x_2). \quad (2.2)$$

With the use of (2.1), the position vector $\mathbf{r}^* = x_i \mathbf{e}_i$ to any point in the fluid can be expressed as a function of the coordinates ζ^i as

$$\begin{aligned} \mathbf{r}^* &= \zeta^1 \mathbf{e}_1 + (R + \zeta^2) \cos(\zeta^3/R) \mathbf{e}_2 + (R + \zeta^2) \sin(\zeta^3/R) \mathbf{e}_3 \\ &= \zeta^1 \mathbf{a}_1 + (R + \zeta^2) \mathbf{a}_2, \end{aligned} \quad (2.3)$$

where \mathbf{a}_1 and \mathbf{a}_2 are defined by

$$\mathbf{a}_1 = \mathbf{e}_1, \quad \mathbf{a}_2 = \cos(\zeta^3/R) \mathbf{e}_2 + \sin(\zeta^3/R) \mathbf{e}_3. \quad (2.4)$$

Further, an orthonormal set of basis \mathbf{a}_i can be defined by introducing

$$\mathbf{a}_3 = \mathbf{a}_1 \times \mathbf{a}_2 = -\sin(\zeta^3/R) \mathbf{e}_2 + \cos(\zeta^3/R) \mathbf{e}_3. \quad (2.5)$$

The base vectors \mathbf{g}_i , the reciprocal basis \mathbf{g}^i and the determinant g of the metric tensor $\mathbf{g}_i \cdot \mathbf{g}_j$, associated with the curvilinear coordinates ζ^i are:

$$\begin{aligned} \mathbf{g}_1 &= \mathbf{a}_1, \quad \mathbf{g}_2 = \mathbf{a}_2, \quad \mathbf{g}_3 = ((R + \zeta^2)/R) \mathbf{a}_3, \quad \mathbf{g}^1 = \mathbf{a}_1, \quad \mathbf{g}^2 = \mathbf{a}_2, \\ \mathbf{g}^3 &= (R/(R + \zeta^2)) \mathbf{a}_3, \quad g^{1/2} = [\mathbf{g}_1 \mathbf{g}_2 \mathbf{g}_3] = (R + \zeta^2)/R. \end{aligned} \quad (2.6)$$

In terms of the curvilinear coordinates (ζ^i) , cross sections of the pipe correspond to fixed values of ζ^3 , and its lateral surface can be represented by

$$(\zeta^1)^2/a^2 + (\zeta^2)^2/b^2 = 1. \quad (2.7)$$

We recall that the steady and fully developed flows must satisfy the two conditions

$$\frac{\partial \mathbf{v}^*}{\partial t} = 0, \quad \frac{\partial}{\partial \zeta}(\mathbf{v}^* \cdot \mathbf{a}_i) = 0, \quad (2.8)$$

respectively, where \mathbf{v}^* denotes the velocity vector in the three-dimensional theory. Moreover, we restrict attention to flows which are symmetric about the ζ^2 – ζ^3 plane so that \mathbf{v}^* must also satisfy the conditions

$$\left. \begin{aligned} \mathbf{v}^*(\zeta^1, \zeta^2, \zeta) \cdot \mathbf{a}_1 &= -\mathbf{v}^*(-\zeta^1, \zeta^2, \zeta) \cdot \mathbf{a}_1, \\ \mathbf{v}^*(\zeta^1, \zeta^2, \zeta) \cdot \mathbf{a}_2 &= \mathbf{v}^*(-\zeta^1, \zeta^2, \zeta) \cdot \mathbf{a}_2, \\ \mathbf{v}^*(\zeta^1, \zeta^2, \zeta) \cdot \mathbf{a}_3 &= \mathbf{v}^*(-\zeta^1, \zeta^2, \zeta) \cdot \mathbf{a}_3, \end{aligned} \right\} \quad (2.9)$$

where we have replaced ζ^3 by ζ in (2.9) and adopt this notation in the rest of the paper. The conditions (2.9) ensure that the component $\mathbf{v}^* \cdot \mathbf{a}_1$ is odd in ζ^1 , while $\mathbf{v}^* \cdot \mathbf{a}_2$ and $\mathbf{v}^* \cdot \mathbf{a}_3$ are even in ζ^1 . Further, we specify the no-slip condition at the wall of the pipe so that \mathbf{v}^* must vanish on the lateral surface (2.7) of the fluid, i.e.

$$\mathbf{v}^*(\zeta^1, \zeta^2, \zeta) = 0 \quad \text{on the surface (2.7)}. \quad (2.10)$$

Now let the moving curve c (of the directed curve \mathcal{R}_K in §2 of Part I) coincide at the current time t with a fixed curve \bar{c} , which we identify here with the centre-line of the circular curved pipe (figure 1). The position vector $\bar{\mathbf{r}}$ of \bar{c} can then be specified by

$$\bar{\mathbf{r}} = R\mathbf{a}_2 \quad (2.11)$$

and the tangent vector $\bar{\mathbf{a}}_3$ to (2.11), calculated from (2.4)₁ of Part I, by virtue of (2.4) and (2.5) is easily seen to be the same as \mathbf{a}_3 . Also, by (2.4)₂ of Part I, the value of $\bar{a}_{33} = 1$. Before proceeding further, it is necessary to make some comments regarding the basic notations to be adopted in Part II. We recall that in §2 of Part I, the eulerian representation of the various basic equations (see, for example, (2.13*a*, *b*)–(2.16) of Part I) utilize the same symbols as in the lagrangian representation but with an added overbar, e.g., $\bar{\mathbf{r}}$ in (2.5) and $(\bar{\lambda}, \bar{y}_{MN}, \bar{\mathbf{d}}_N, \bar{w}_N)$ in (2.13*b*)–(2.16) of Part I. In the interest of simplicity, however, in the remainder of Part II, we record the eulerian forms of the various results without the overbar. This should not cause any difficulty since only the eulerian form of the theory is used in Part II.

As will become evident later, for the particular application under discussion and in anticipation of the calculations to be executed on a fairly complex algebraic system of equations, the choice of the weighting functions and the specification of the constitutive coefficients in the direct theory can be facilitated by employing a slightly different (but equivalent) notation than that in §2 of Part I. In this connection, we observe that in the formulation of the basic theory in (Part I, §2) an index N ($N = 1, 2, \dots, K$) was used to designate any number of directors and other related kinematical and kinetical variables. Alternatively, we may utilize a somewhat different labelling that involves a dual index of the form

$$\mathbf{d}_N^i, \quad \mathbf{w}_N^i, \quad \mathbf{k}_N^i, \quad \mathbf{m}_N^i, \quad \text{etc.} \quad (N = 1, 2, \dots), \quad (2.12)$$

where the index i takes the value 1, 2, 3 only. The scheme used in the formulation of the basic theory in (Part I, §2) can be arranged to be equivalent to that indicated in (2.12), but the latter to be adopted here easily permits identification of multiples of three entities and thus provides some notational advantages in computation. Clearly, the basic theory in (Part I, §2) can also be formulated in terms of the indexing scheme of (2.12) simply by replacing the index N with the dual index i_N in a manner displayed in (2.12). In particular, in terms of this notational scheme, the expression (A 11) in Part I for the present purpose can be rewritten in the form

$$\mathbf{v}^* = \mathbf{v}^*(\zeta^1, \zeta^2, \zeta, t) = \mathbf{v}(\zeta, t) + \sum_{N=1}^K \lambda_N^i(\zeta^1, \zeta^2) \mathbf{w}_N^i(\zeta, t), \quad (2.13)$$

where the usual convention for summation over the repeated lower case Latin index i is understood. Referred to the basis \mathbf{a}_i , the various kinematical and kinetical variables occurring in the basic equations (2.13a)–(2.16) of Part I now read as

$$\left. \begin{aligned} \mathbf{v} &= v_i \mathbf{a}_i, & \mathbf{w}_N^i &= w_{Nj}^i \mathbf{a}_j, & \mathbf{n} &= n_i \mathbf{a}_i, & \mathbf{k}_N^i &= k_{Nj}^i \mathbf{a}_j, \\ \mathbf{m}_N^i &= m_{Nj}^i \mathbf{a}_j, & \mathbf{f} &= f_i \mathbf{a}_i, & \mathbf{l}_N^i &= l_{Nj}^i \mathbf{a}_j. \end{aligned} \right\} \quad (2.14)$$

The condition of incompressibility in the three-dimensional theory (see also Part I, the paragraph containing (3.5)) when expressed in terms of the curvilinear coordinates ζ^i and the associated base vectors (2.6), after using the representation (2.13) for \mathbf{v}^* can be expressed in the form

$$v_{3,\zeta} + \sum_{N=1}^K \{ (R + \zeta^2) \lambda_{N,1}^i w_{N1}^i + [(R + \zeta^2) \lambda_N^i]_{,2} w_{N2}^i + \lambda_N^i w_{N3,\zeta}^i \} = 0, \quad (2.15)$$

where in (2.15) a comma indicates partial differentiation. One way that a velocity field such as (2.13) can meet the requirement of incompressibility is to choose the weighting functions λ_N^i such that (2.15) is identically satisfied. To elaborate, consider the quantity in the brackets $\{ \}$ of the series portion of (2.15), which (in view of the implied summation over i) can be displayed as

$$\begin{aligned} & \underline{(R + \zeta^2) \lambda_{N,1}^1 w_{N1}^1 + (R + \zeta^2) \lambda_{N,1}^2 w_{N1}^2 + (R + \zeta^2) \lambda_{N,1}^3 w_{N1}^3} \\ & + [(R + \zeta^2) \lambda_N^1]_{,2} w_{N2}^1 + \underline{[(R + \zeta^2) \lambda_N^2]_{,2} w_{N2}^2 + [(R + \zeta^2) \lambda_N^3]_{,2} w_{N2}^3} \\ & + \lambda_N^1 w_{N3,\zeta}^1 + \lambda_N^2 w_{N3,\zeta}^2 + \lambda_N^3 w_{N3,\zeta}^3. \end{aligned} \quad (2.16)$$

If the first term on the left-hand side of (2.15) is zero and also if the expression (2.16) vanishes for each N , then (2.15) is identically satisfied. But even with this relatively simple scheme, there are a variety of ways that the vanishing of (2.16) can be effected. To see this, suppose that w_{N1}^1 and w_{N2}^2 are equal so that the terms underlined in (2.16) combine to yield the expression

$$\{ (R + \zeta^2) \lambda_{N,1}^1 + [(R + \zeta^2) \lambda_N^2]_{,2} \} w_{N1}^1. \quad (2.17)$$

Now if (2.17) vanishes and if all components of w_{Nj}^i ($i, j = 1, 2, 3$) except w_{N1}^1 and w_{N2}^2 are zero, then the satisfaction of (2.15) is ensured provided the weighting functions λ_N^1 and λ_N^2 are chosen such that

$$\text{Coefficient of } w_{N1}^1 \text{ in (2.17)} = 0. \quad (2.18)$$

Although the discussion between (2.15)–(2.18) could be regarded only as an illustration by means of which the incompressibility condition can be satisfied, the

choices suggested in the preceding paragraph can be actually motivated with reference to the problem of flow in a curved pipe as follows: (1) the vanishing of the gradient with respect to ζ of the velocity \mathbf{v} and the director velocities \mathbf{w}_N^i readily guarantee the satisfaction of the condition (2.8)₂ for fully developed flow; (2) the equality of w_{N1}^1 and w_{N2}^2 is motivated by the fact that the velocity components in the cross-flow directions \mathbf{a}_α ($\alpha = 1, 2$ only) are equal so that the requirement (2.18) corresponds to a part of incompressibility due to cross-flow velocities; and (3) finally setting in (2.15) some of the components of the director velocities equal to zero still allows for the specification of a fairly general set of weighting functions in the representation (2.13) and at the same time will result in a simpler system of equations of motion.

Keeping the background information of the preceding paragraph in mind, we now set

$$\left. \begin{aligned} v_{3,\zeta} = w_{N3,\zeta}^1 = 0, \quad w_{N3,\zeta}^2 = 0, \quad w_{N3,\zeta}^3 = 0, \\ w_{N1}^1 = w_{N2}^2, \quad w_{N2}^1 = 0, \quad w_{N1}^3 = 0, \quad w_{N1}^2 = 0, \quad w_{N2}^3 = 0, \end{aligned} \right\} \quad (2.19)$$

which represent constraints that arise from the incompressibility condition (2.15). In addition, without loss in generality, we also set

$$\mathbf{v} = 0, \quad w_{N3}^1 = 0, \quad w_{N3}^2 = 0. \quad (2.20)$$

The first of the additional constraints (2.20) is based on the fact that a term such as \mathbf{v} in (2.13) can be represented by any one of the series terms (with an appropriate value for the accompanying weighting function), while the motivation for (2.20)_{2,3} is due to (2.19)_{2,3} according to which the gradient with respect to ζ of the cross-flow velocities is zero and hence w_{N3}^1 and w_{N3}^2 are necessarily constants and may be set equal to zero. It should be emphasized, however, that even though by (2.19)₄ the gradient with respect to ζ of the axial component of the velocity vanishes, it would be much too restrictive to set w_{N3}^3 equal to zero since this would preclude the case of uniform flow.

In line with the discussion of constraints in (Part I, last paragraph of §2), indeterminacies associated with the constraints (2.19) and (2.20) arise in the constitutive equations for the kinetical quantities \mathbf{n} , \mathbf{k}_N^i and \mathbf{m}_N^i . Keeping this in mind, the full constitutive equations for the kinetical variables are:

$$\begin{aligned} \mathbf{n} &= \mathbf{n}_{\text{ind}}, \\ \mathbf{m}_N^1 &= -(r_N \mathbf{a}_1 + \bar{r}_{N2}^1 \mathbf{a}_2 + \bar{r}_{N3}^1 \mathbf{a}_3) + \hat{\mathbf{m}}_N^1, \\ \mathbf{m}_N^2 &= -(r_N \mathbf{a}_2 + \bar{r}_{N2}^2 \mathbf{a}_1 + \bar{r}_{N3}^2 \mathbf{a}_3) + \hat{\mathbf{m}}_N^2, \\ \mathbf{m}_N^3 &= -(p_N \mathbf{a}_3 + \bar{p}_{N1} \mathbf{a}_1 + \bar{p}_{N2} \mathbf{a}_2) + \hat{\mathbf{m}}_N^3, \end{aligned} \quad (2.21)$$

and

$$\begin{aligned} \mathbf{k}_N^i &= -(r_{N2}^1 \mathbf{a}_2 + r_{N3}^1 \mathbf{a}_3 + q_N \mathbf{a}_1) + \hat{\mathbf{k}}_N^1, \\ \mathbf{k}_N^2 &= -\left(r_{N1}^2 \mathbf{a}_1 + r_{N3}^2 \mathbf{a}_3 - \frac{\bar{r}_{N3}^2}{R} \mathbf{a}_2 - \frac{r_N}{R} \mathbf{a}_3 - q_N \mathbf{a}_2\right) + \hat{\mathbf{k}}_N^2, \\ \mathbf{k}_N^3 &= -\left(p_{N1} \mathbf{a}_1 + p_{N2} \mathbf{a}_2 + \frac{\bar{p}_{N2}}{R} \mathbf{a}_3\right) + \hat{\mathbf{k}}_N^3, \end{aligned} \quad (2.22)$$

where the indeterminate parts r_N , q_N , p_N , r_{Nj}^i , \bar{r}_{Nj}^i , p_{Ni} , \bar{p}_{Ni} are arbitrary functions of ζ, t and the determinate parts $\hat{\mathbf{m}}_N^i$, $\hat{\mathbf{k}}_N^i$ are to be specified by constitutive equations.

Before substitution of equations (2.21) and (2.22) into the eulerian representation of the equations of motion (see (2.14) of Part I), it is convenient to introduce the abbreviation \mathbf{b}_N^i for the sum of the series in (2.14) of Part I after using also the dual index notation in (2.14) with $N = 1, 2, \dots, K$, namely

$$\mathbf{b}_N^i = \lambda \sum_{M=0}^K \left(y_{MN}^{ij} \frac{\partial \mathbf{w}_M^j}{\partial t} + v_{MN}^{ij} \frac{\partial \mathbf{w}_M^j}{\partial \zeta} + u_{MN}^{ij} \mathbf{w}_M^j \right). \quad (2.23)$$

The various symbols in (2.23) are defined by the expressions (A 20) in Appendix A of Part I, apart from the deletion of the overbar noted at the end of the third paragraph of this section containing (2.11). With the use of (2.23), the equations of motion of Part I can be rewritten as

$$\partial \mathbf{n} / \partial \zeta = \lambda (\mathbf{b}_0 - \mathbf{f}) \quad (2.24)$$

$$\text{and} \quad \partial \mathbf{m}_N^i / \partial \zeta - \mathbf{k}_N^i = \lambda (\mathbf{b}_N^i - \mathbf{l}_N^i) \quad (N = 1, 2, \dots, K), \quad (2.25)$$

where in writing (2.24) we have kept in mind the dual index notations indicated earlier in this section.

We set (2.24) temporarily aside and substitute the expressions (2.21) and (2.22) in the equations of motion (2.25). Then, taking the \mathbf{a}_3 -component of the resulting equation with $i = 3$ and adding the \mathbf{a}_1 -component with $i = 1$ to the \mathbf{a}_2 -component with $i = 2$, we are led to the following two equations:

$$\left. \begin{aligned} -p_{N,\zeta} + \hat{m}_{N3,\zeta}^3 + \hat{m}_{N2}^3/R - \hat{k}_{N3}^3 &= \lambda (b_{N3}^3 - l_{N3}^3), \\ (\hat{m}_{N1}^1 + \hat{m}_{N2}^2)_{,\zeta} - \hat{m}_{N3}^2/R - (\hat{k}_{N1}^1 + \hat{k}_{N2}^2) &= \lambda (b_{N1}^1 + b_{N2}^2 - l_{N1}^1 - l_{N2}^2). \end{aligned} \right\} \quad (2.26)$$

The first of (2.26) contains only the constraint response p_N , while the second of (2.26) is entirely free from constraint responses. The remaining components of the system (2.24) and (2.25) can be regarded as the equations for the determination of the constrained responses $(\mathbf{n})_{\text{ind}}$, r_{Nj}^i , \bar{r}_{Nj}^i , p_{Ni} , \bar{p}_{Ni} , r_N and q_n and are not needed in the subsequent analysis.

It follows from the foregoing developments that for the problem of flow in a curved pipe under discussion, we only need to consider (2.26) as the relevant equations of motion. For a complete theory, constitutive equations are required for the determinate parts $\hat{\mathbf{m}}_N^i$, $\hat{\mathbf{k}}_N^i$ and the inertia coefficients which occur in (2.23). We note that these constitutive equations can be specified by integration of known constitutive relations in the exact three-dimensional theory, as discussed in Part I (Appendix A, especially the expressions (A 28)–(A 31)). These expressions for $\hat{\mathbf{m}}_N^i$, $\hat{\mathbf{k}}_N^i$, \mathbf{f} , \mathbf{l}_N^i can be readily calculated from the last four of (A 30) in Part I. Similarly, the inertia coefficients can be evaluated from (A 28) and the last three of (A 20) in Part I. We defer the specification of the pressure gradient $p_{N,\zeta}$ in (2.26)₁ which can be determined from the corresponding solution for a straight pipe of an elliptical cross section.

Before closing this section, we observe that in view of the choice (2.20)₁, namely $\mathbf{v} = \mathbf{0}$, and after an appeal to the conditions (2.8)_{1,2} for steady and fully developed flow, the expression (2.13) can be reduced to the form

$$\mathbf{v}^* = \sum_{N=1}^K \lambda_N^i(\zeta^1, \zeta^2) w_{Nj}^i \mathbf{a}_j, \quad (2.27)$$

with the components $w_{Nj}^i = w_N^i \cdot a_j$ (2.28)

of the director velocities being constants, independent of ζ and t .

3. Choice of the weighting functions associated with an hierarchical structure of the theory

Before the use of the relevant system of equations consisting of the primitive equations of motion (2.26), the conservation of mass (see (2.13*b*) of Part I) and the appropriate constitutive equations, it is necessary to choose the weighting functions $\lambda_N^i(\zeta^1, \zeta^2)$ in (2.27). Clearly, a judicious choice of these weighting functions can reduce the complexity of the system of equations in the direct formulation of the theory. Moreover, the choice of λ_N^i should be consistent with the hierarchical structure of the basic theory (see the remarks in §2 of Part I, the paragraph following (2.22)) so that the equations for each hierarchy include the equations of all lower hierarchies.

Given that the choice of the weighting functions for the curved pipe is more difficult than the corresponding choice for a straight pipe (see, for example, §3 of Part I), it is desirable to provide here some motivation for the choice of λ_N^i . For this purpose, we first recall that the relationship between the number H identifying the order of hierarchical theory and the number of directors (in the basic theory of the type constructed in §2 of Part I) at each hierarchical level is (Naghdi 1982, §9):

$$\frac{1}{2}H(H+3) \quad (H = 1, 2, \dots). \quad (3.1)$$

(The expression (3.1) corresponds to the right-hand side of (9.1) in Naghdi (1982, p. 85), where a different symbol is used to designate the hierarchical level.) Setting aside temporarily the expression (2.27) but keeping in mind as background its functional dependence with components (2.28) of the director velocities as constants, we consider a particular hierarchical representation of order H for the velocity \mathbf{v}^* in the form

$$\mathbf{v}^* = \sum_{j=0}^H \sum_{i=0}^j (\zeta^1)^i (\zeta^2)^{j-i} a_{ij}^k \mathbf{a}_k, \quad (3.2)$$

where the coefficients a_{ij}^k are constants and summation is implied over the values of the index k . (An expression such as (3.2) may be regarded as a truncation of an exact expression to the kinematical variable in the three-dimensional theory; and, as will become evident later, the development between (3.2)–(3.4) will serve as physical motivation of the main objective in this section.) Clearly the form (3.2) fulfils the requirements (2.8)_{1,2} and it remains to satisfy the flow symmetry conditions (2.9), the no-slip condition (2.10) and the incompressibility condition which when referred to the curvilinear coordinates $(\zeta^1, \zeta^2, \zeta)$ reads as

$$v_{1,1}^* + v_{2,2}^* + v_2^*/(R + \zeta^2) = 0, \quad (3.3)$$

with the velocity components in (3.3) being

$$v_1^* = \mathbf{v}^* \cdot \mathbf{a}_1, \quad v_2^* = \mathbf{v}^* \cdot \mathbf{a}_2.$$

After substituting (3.2) into (2.9), (2.10) and (3.3), and using the resulting conditions to eliminate some of the coefficients a_{ij}^k in (3.2), the expression for \mathbf{v}^* can be displayed as

$$\mathbf{v}^* = \sum_{N=1}^L (\lambda_N^1 c_N^1 \mathbf{a}_1 + \lambda_N^2 c_N^2 \mathbf{a}_2) + \sum_{N=1}^K \lambda_N^3 c_N^3 \mathbf{a}_3, \quad c_N^1 = c_N^2, \quad (3.4)$$

Table 1

index N of weights in (3.7)	exponent i_N	exponent j_N
1	0	0
2	0	1
3	0	2
4	2	0
5	0	3
6	2	1
7	0	4
8	2	2
9	4	0
10	0	5
11	2	3
12	4	1

where the constant coefficients c_N^1 are linear combinations of a_{ij}^k and the quantities $\lambda_N^{i_N}$ are polynomials in ζ^1, ζ^2 given by

$$\left. \begin{aligned} \lambda_N^1 &= \frac{a}{b} \left(1 + \frac{\zeta^2}{R} \right) \mu_1 \left(\frac{\zeta^1}{a} \right)^{i_N+1} \left(\frac{\zeta^2}{b} \right)^{j_N-1} \left[4 \left(\frac{\zeta^2}{b} \right)^2 - j_N \mu_1 \right] - 2 \frac{a}{R} \mu_1^2 \left(\frac{\zeta^1}{a} \right)^{i_N+1} \left(\frac{\zeta^2}{b} \right)^{j_N}, \\ \lambda_N^2 &= - \left(1 + \frac{\zeta^2}{R} \right) \mu_1 \left(\frac{\zeta^1}{a} \right)^{i_N} \left(\frac{\zeta^2}{b} \right)^{j_N} \left[4 \left(\frac{\zeta^1}{a} \right)^2 - (i_N + 1) \mu_1 \right], \\ \lambda_N^3 &= \mu_1 (\zeta^1/a)^{i_N} (\zeta^2/b)^{j_N}, \end{aligned} \right\} \quad (3.5)$$

$$\text{where} \quad \mu_1 = 1 - (\zeta^1/a)^2 - (\zeta^2/b)^2. \quad (3.6)$$

To continue the discussion, it is clear that the use of $(3.4)_2$ would simplify somewhat the first series term on the right-hand side of (3.4). However, at this point, it is best not to invoke $(3.4)_2$ which may be viewed as corresponding to the condition $(2.19)_5$. The exponents in (3.5) involve the integers i_N and j_N which depend on the index N of the weighting functions and this relationship is illustrated in table 1 for a few values of N .

An examination of table 1 reveals a definite pattern of a relationship between i_N , j_N and N , which can be easily summarized by the following algorithm.

$$\left. \begin{aligned} (1) \quad & \text{Find the unique integer } Q \text{ such that the index } N \text{ has a value} \\ & \text{between } Q(Q-1)+1 \text{ and } Q(Q+1), \text{ i.e.} \\ & \quad Q(Q-1)+1 \leq N \leq Q(Q+1), \\ (2) \quad & \text{then, if } N \leq Q^2, \text{ let } P = N - Q(Q-1) - 1, \text{ and define } i_N = 2P \\ & \text{and } j_N = 2(Q-P-1), \\ (3) \quad & \text{then, if } N > Q^2, \text{ let } P = N - Q^2 - 1, \text{ and define } i_N = 2P \\ & \text{and } j_N = 2(Q-P) - 1. \end{aligned} \right\} \quad (3.7)$$

We comment briefly on how the results of the reduction process outlined between (3.2)–(3.7) were effected. using the computer program *VAXIMA*, the algebraic manipulation described above was carried out for hierarchies of several order ($H = 3$ to $H = 12$). (A more detailed description of this program is indicated at the end of §1c.) The form of the equations (3.5) was determined by induction after observing a definite pattern in the results of the reduction as H was increased.

Before indicating the relationship between the expression (2.27) and (3.4)–(3.5), it is important to observe several features of the representation (3.4). Advantages of the dual index scheme introduced in §2 is now evident from a close examination of (3.4)₁, where a superscript index serves to designate a corresponding coordinate direction so that λ_N^1, λ_N^2 are the weights for the cross-flow and λ_N^3 are the weights for the axial-flow. Additionally, the number of terms representing the cross- and the axial-flows are different. These are designated (see the upper limits in the summation signs of (3.4)) by L and K , respectively, which are determined by the order of hierarchy H as follows:

$$K = \begin{cases} \frac{1}{2}(\frac{1}{2}H^2) & \text{for even } H, \\ \frac{1}{2}(\frac{1}{2}(H^2-1)) & \text{for odd } H, \end{cases} \quad L = \begin{cases} 0 & \text{for } H < 5, \\ \frac{1}{2}(\frac{1}{2}((H-3)^2-1)) & \text{for even } H, \\ \frac{1}{2}(\frac{1}{2}(H-3)^2) & \text{for odd } H. \end{cases} \quad (3.8)$$

It should be noted here that in the basic hierarchical theory of order H in §2 of Part I or similar earlier works as discussed in Naghdi (1982, §§9–13), the weighting functions were not subjected to boundary or special conditions, while in the present paper the choice of the weighting functions is made after imposing the restriction (2.8), (2.9), (2.10) and the incompressibility condition (3.3) on (3.2). Thus, for a given hierarchical order H , the number of the weighting functions in the original primitive equations would be different from those in (3.4). More specifically for a given H , the number of weighting functions in §2 of Part I is given by (3.1) while the corresponding number of the weighting functions (or the number of director velocity vectors) here is

$$K + L = \frac{1}{2}H(H-3) + 2. \quad (3.9)$$

Having disposed of the development and the discussion between (3.2)–(3.9), we now proceed to indicate the relationship of (2.27) to (3.4). Expanding the sum on i and j in (2.27) and appealing to the constraint conditions (2.19) and (2.20), (2.27) can be reduced to

$$v^* = \sum_{N=1}^K \lambda_N^1 w_{N1}^1 a_1 + \lambda_N^2 w_{N2}^2 a_2 + \lambda_N^3 w_{N3}^3 a_3. \quad (3.10)$$

The expression (3.10) has the same form as (3.4)₁, apart from the fact that the summation over the index N in (3.4)₁ by virtue of (3.8) involves K weights for the axial flow and L ($L < K$) weights for the cross-flow. However, this notational difference can be easily adjusted by setting

$$\lambda_N^1 = \lambda_N^2 = 0 \text{ only for values of } N > L \text{ or } N = L+1, L+2, \dots, K, \quad (3.11)$$

where K and L are defined by (3.8). With the stipulation (3.11), which also meets all the requirements (2.8)–(2.10) and the incompressibility, without loss in generality we may replace in (2.27), or equivalently (3.10) the summation from $N = 1, \dots, K$ by $N = 1, \dots, L$, with K and L given by (3.8); and, after the trivial identification of w_{N1}^1 with c_N^1 , w_{N2}^2 with c_N^2 , etc., 1–1 correspondence exists between (3.4)₁ and (3.10). It then follows that (2.27), or equivalently (3.10) can be rewritten in terms of (3.5) and our task for the choice of the weighting functions is complete.

4. Reduction of the equations of motion of the direct theory

We obtain in this section a reduced form of the equations of the direct theory for steady flow in curved pipes, after substitution of the weighting functions and explicit forms of the constitutive equations into (2.26) and other relevant equations.

Let x, y, z (not to be confused with similar frequently adopted notation for a rectangular cartesian coordinate system) denote dimensionless variables defined by

$$x = \zeta^1/a, \quad y = \zeta^2/b, \quad z = \zeta/b. \quad (4.1)$$

Since the various results of interest in §§2 and 3 involve only the components $w_{N1}^1, w_{N2}^2, w_{N3}^3$ of the director velocities, we define their corresponding dimensionless forms as

$$X_N = -\frac{Re_0}{2w_0} w_{N1}^1 = -\frac{Re_0}{2w_0} w_{N2}^2, \quad B_N = \frac{1}{2w_0} w_{N3}^3. \quad (4.2)$$

In (4.2), w_0 stands for a characteristic speed which in anticipation of later results will be identified as the average axial velocity in a straight pipe of the same elliptical cross section, and Re_0 is the corresponding Reynolds number defined by

$$Re_0 = 2\rho^*bw_0/\mu, \quad (4.3)$$

where μ is the coefficient of shear viscosity and ρ^* is a constant mass density of the fluid in the three-dimensional theory. In terms of (4.1), the aspect ratio, i.e. the ratio of the minor to major axes of the elliptical cross section

$$\epsilon = b/a, \quad (4.4)$$

and the curvature ratio δ introduced in (1.1), the weighting functions (3.5) and the expression (3.6) can now be recorded as

$$\left. \begin{aligned} \lambda_N^1 &= \epsilon^{-1}(1+\delta y)\mu_1 x^{i_{N+1}} y^{j_{N-1}} [4y^2 - j_N \mu_1] - 2(\delta/\epsilon)\mu_1^2 x^{i_{N+1}} y^{j_N}, \\ \lambda_N^2 &= -(1+\delta y)\mu_1 x^{i_N} y^{j_N} [4x^2 - (i_N+1)\mu_1], \\ \lambda_N^3 &= \mu_1 x^{i_N} y^{j_N} \end{aligned} \right\} \quad (4.5)$$

$$\text{and} \quad \mu_1 = 1 - x^2 - y^2. \quad (4.6)$$

We also define here the dimensionless forms of the Lagrange multipliers p_N and their gradients which occur in (2.26)₁ by

$$\bar{p}_N = p_N/2\mu a w_0, \quad \bar{p}'_N = \bar{p}_{N,z}, \quad (4.7)$$

where ()' denotes differentiation with respect to the variable z in (4.1).

An outline of the calculations of the inertia coefficients $y_{MN}^{ij}, v_{MN}^{ij}, u_{MN}^{ij}$ in (2.23) using the dual index scheme indicated in (2.12), and an explicit determination of the relevant constitutive equations for the components of \hat{m}_N^i and \hat{k}_N^i which occur in (2.26) is already indicated in §2 (the paragraph before last). These constitutive results, which represent fairly complex expressions when eventually substituted into (2.26) yield a reduced non-dimensionalized form of the equations of motion. The latter system of equations will necessarily involve the shear viscosity μ and the geometrical parameters ϵ and δ defined, respectively, by (4.4) and (1.1). Here we record the non-dimensional version of the reduced equations of motion in the form

$$-\bar{p}'_N - \sum_{M=1}^K A_{NM} B_M = \sum_{M=1}^L \sum_{R=1}^K C_{NMR} X_M B_R, \quad (4.8)$$

$$\text{and} \quad -\sum_{M=1}^L D_{NM} X_M = \sum_{M=1}^L \sum_{R=1}^L E_{NMR} X_M X_R + \kappa_0^2 \sum_{M=1}^K \sum_{R=1}^K F_{NMR} B_M B_R, \quad (4.9)$$

where we have also introduced a Dean number κ_0 by

$$\kappa_0 = \delta^{\frac{1}{2}} Re_0. \quad (4.10)$$

(The quantity defined by (4.10) and based on (4.3) arises naturally at this stage of our theoretical development, although it can be subsequently related to the Dean number κ defined by (1.3) and frequently used in the presentation of the experimental data.)

The dimensionless constitutive coefficients A_{NM} , C_{NMR} , D_{NM} , E_{NMR} and F_{NMR} in (4.8) and (4.9) are recorded in Appendix A which also contains an outline of the manner in which the coefficients are calculated. Also, the upper limits over the summation signs in (4.8) and (4.9) reflect the choice made in §3 of different numbers of the weighting functions indicated in (3.8), which accompany the director velocities in axial- and cross-flow directions.

Let the components of the velocity field (3.10) referred to the orthonormal basis \mathbf{a}_i (defined in (2.4) and (2.5)) be designated by $v_i^* = \mathbf{v}^* \cdot \mathbf{a}_i$. Then, with the help of (4.2) and (4.5), the dimensionless form of these velocity components can be written as

$$\left. \begin{aligned} v_1^* &= -\frac{2w_0}{\epsilon Re_0} \sum_{N=1}^L \mu_1 x^{i_{N+1}} y^{j_{N-1}} [(1+\delta y)(4y^2 - j_N \mu_1) - 2\delta \mu_1 y] X_N, \\ v_2^* &= \frac{2w_0}{Re_0} \sum_{N=1}^L (1+\delta y) \mu_1 x^{i_N} y^{j_N} [4x^2 - (i_N + 1) \mu_1] X_N, \\ v_3^* &= 2w_0 \sum_{N=1}^K \mu_1 x^{i_N} y^{j_N} B_N. \end{aligned} \right\} \quad (4.11)$$

The mean axial speed w along the pipe may be obtained by integrating (4.11)₃ over the elliptical cross section and dividing by the area πab of the cross section so that

$$w = \frac{1}{\pi ab} \iint_A v_3^* da = w_0 \sum_{N=1}^K 4\alpha_{10}^{i_N j_N} B_N, \quad (4.12)$$

where the values of the coefficient $\alpha_{10}^{i_N j_N}$ can be calculated from (A 2) of Appendix A.

In anticipation of a comparison in the next section of the velocity field predicted by the expressions (4.11) with corresponding recent numerical results obtained from the Navier–Stokes equations, we introduce now a scalar function ψ by

$$\psi = \frac{2w_0}{Re_0} \sum_{L=1}^K (1+\delta y)^2 \mu_1^2 x^{i_{N+1}} y^{j_N} X_N, \quad (4.13)$$

the right-hand side of which involves only the dimensionless cross-flow velocities defined in (4.2). By differentiating (4.13) with respect to the dimensionless variables (4.1)_{1,2}, it can be readily verified that the cross-flow velocities (4.11)_{1,2} are related to (4.13) through the relations

$$v_1^* = -\frac{1}{\epsilon} \left(\frac{\psi}{1+\delta y} \right)_{,y}, \quad v_2^* = \left(\frac{\psi}{1+\delta y} \right)_{,x}, \quad (4.14)$$

which are similar to the expressions for the velocity components in terms of a stream function in the three-dimensional theory. This similarity is even more apparent if we write $\psi = (1+\delta y) \bar{\psi}$ in which case one immediately obtains

$$\epsilon v_1^* = -\bar{\psi}_{,y}, \quad v_2^* = \bar{\psi}_{,x}.$$

We close this section by indicating the nature of specialization of the main results for the case of a straight pipe of circular cross section. In this case, $\delta = 0$, $\epsilon = 1$ and

it follows from the definition (4.10) that $\kappa_0 = 0$. A solution for the steady, fully developed, flow in a straight pipe of circular cross section is the well-known Poiseuille flow. In the context of the direct theory used here, this solution can be obtained from the system of nonlinear equations (4.8) and (4.9) by setting

$$\left. \begin{aligned} B_1 &= 1, & B_M &= 0, & M &= 2, \dots, K, \\ X_M &= 0, & M &= 1, \dots, L, \\ \bar{p}'_M &= -A_{M1}, & M &= 1, \dots, K. \end{aligned} \right\} \quad (4.15)$$

In particular, after substituting (4.15) into (4.11), we obtain

$$v_1^* = v_2^* = 0, \quad v_3^* = 2w_0\mu_1, \quad (4.16)$$

which with the help of (4.6) can be easily shown to be the same as the corresponding solution in the three-dimensional theory if w_0 in the present development is identified with the average axial velocity in the straight pipe.

The solution of (4.8) and (4.9) for the same pressure gradient as that of Poiseuille flow (see the last of (4.15)) can then be used to calculate the friction loss factor defined earlier in §1*a*. For this purpose, recalling (1.5), (1.4), and the definition w_0 given following (4.2), we note that the friction loss factor can be expressed as the ratio $f = Q_s/Q_c = w_0/w$ or as

$$1/f = \kappa/\kappa_0, \quad (4.17)$$

in view of (1.3) and (4.10). Then, by (4.17) and (4.12) we have

$$f = 1 \left/ \sum_{N=1}^K G_N B_N \right., \quad (4.18)$$

where $G_N = 4\alpha_{10}^{j_N}$. We are now in a position to rewrite the equations of motion (4.8) and (4.9) for pipes of circular cross section in terms of κ (rather than κ_0) using also the result (4.18) as follows:

$$\sum_{M=1}^K A_{NM} B_M + \sum_{M=1}^L \sum_{R=1}^K C_{NMR} X_M B_R = A_{N1}, \quad (4.19)$$

$$\left[\sum_{M=1}^L D_{NM} X_M + \sum_{M=1}^L \sum_{R=1}^L E_{NMR} X_M X_R \right] \left(\sum_{Q=1}^K G_Q B_Q \right)^2 + \kappa^2 \sum_{M=1}^K \sum_{R=1}^K F_{NMR} B_M B_R = 0. \quad (4.20)$$

5. Complete solution for circular pipes of circular cross section

For a given hierarchical order H and the associated number of director velocity components K and L (defined by (3.8)), equations of motion of (4.19) and (4.20) form a nonlinear algebraic system of $K+L$ equations for the determination of cross-flow and axial-flow velocity components defined by (4.2). This system of equations, using the temporary abbreviation

$$\mathbf{Y} = \{X_N, B_M\} \quad (5.1)$$

($N = 1, 2, \dots, L$ and $M = 1, 2, \dots, K$) may be displayed symbolically as

$$\mathbf{F}(\mathbf{Y}, \kappa, \delta, \epsilon) = \mathbf{0}. \quad (5.2)$$

The above equation represents $K+L$ vector-valued function \mathbf{F} of $K+L$ real variables \mathbf{Y} with $(\kappa, \delta, \epsilon)$ as parameters.

The aim of this section is to describe the procedure for obtaining a complete solution for a circular pipe of circular cross section from (4.19) and (4.20) or equivalently (5.2). Thus, in the remainder of this section we discuss in separate subsections the iterative method used to solve the system of equations (5.2), the treatment of the singular points in the solution, a procedure for calculation of streamlines and axial velocity contours, and finally the results of the calculations along with extensive comparisons with the experimental data and recent numerical solutions of the same problem obtained from the Navier–Stokes differential equation.

(a) *The procedure for obtaining a complete solution*

The simplest and most effective method for obtaining a solution of (5.2) was found to be that described by Powell (1970), which combines Newton's method and scaled gradient methods. (The implementation of Powell's method here made use of a subroutine available from the Numerical Algorithms Group (U.S.A.) Incorporated, Mark 9, although a FORTRAN version of the algorithm is available in the literature (Powell 1970).) As with any iterative method, an initial estimate of the solution \mathbf{Y} must also be provided for Powell's method. Since it was of interest to solve (5.2) for a range of $\kappa > 0$ and since the solution for $\kappa = 0$ is known, namely the Poiseuille flow given by (4.15), a procedure for specification of the initial estimate is as follows: Increase κ from zero by steps; and use the solution for \mathbf{Y} , obtained at the smaller value of κ , as the initial estimate for \mathbf{Y} at the present value of κ . It should be mentioned, however, that Powell's method has a rather large region of global convergence, larger than Newton's method, and that some success in obtaining the solution for a particular value of κ was realized by specifying random initial estimates for the solution.

(b) *Treatment of singular points of the solution*

In the course of computations by the procedure described in §5a, it became clear that for increasing values of κ , the convergence of Powell's method failed for values of Dean number larger than some value κ_s (for example, $\kappa_s = 1316$ in figure 5). The numerical value of κ_s was found to depend on the hierarchy. Computation of the determinant of the gradient near this point led us to conclude that κ_s was a singular point. A very simple algorithm was found to be quite effective to traverse this singular point which turned out to be a simple fold singularity (Yang & Keller 1986). (This type of singularity or bifurcation is also called a limit point (see Winters & Brindley 1984).) Two successive solutions before the singular point, i.e. \mathbf{Y}_1 at κ_1 and \mathbf{Y}_2 at κ_2 , were used to compute an initial estimate of the solution \mathbf{Y} at an intermediate value of Dean's number $\kappa_1 < \kappa < \kappa_2 < \kappa_s$ by

$$\mathbf{Y} = \mathbf{Y}_2 - \frac{\kappa - \kappa_2}{\kappa_1 - \kappa_2} (\mathbf{Y}_1 - \mathbf{Y}_2). \quad (5.3)$$

The formula (5.3) is simply a secant extrapolation for the estimate \mathbf{Y} which assumes that the graph of $\mathbf{Y}(\kappa)$ is folded at κ_s . This algorithm is a first order continuation scheme similar to the Euler–Newton continuation described by Yang & Keller (1986). Convergence of the numerical scheme was realized with the initial estimate (5.3) whenever the solutions \mathbf{Y}_1 and \mathbf{Y}_2 were 'close' to each other. This same algorithm was successful also for singularities encountered with decreasing values of κ , which occurred for some of the hierarchies as discussed in §5d.

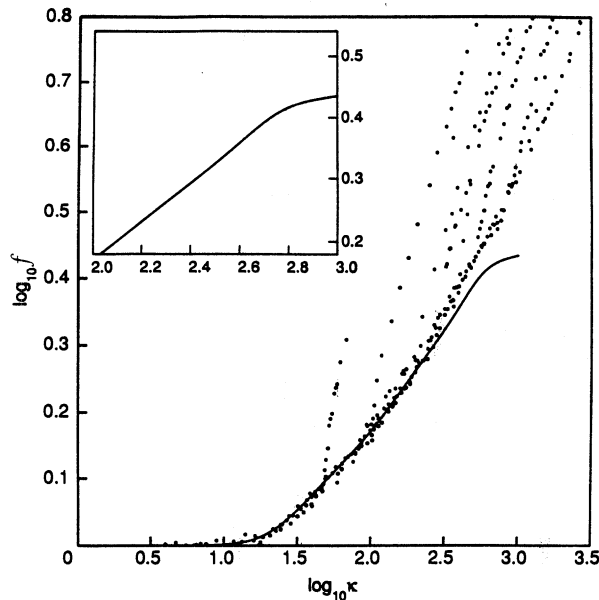


Figure 3. Theoretical prediction of the direct theory for the 8th hierarchy (circular cross section, curvature ratio $\delta = 0.01$) displayed as a solid line for the friction loss in the range $0 < \log \kappa < 3.5$. Also exhibited are the experimental data from Itô (1959) collectively designated by dots. The inset is an enlarged portion of the friction loss curve over the range $2.0 < \log \kappa < 3.0$.

(c) *A procedure for calculation of the streamlines and axial velocity contours*

The streamlines were calculated by finding level curves of the stream function (4.13), i.e. $\psi = \psi(x, y) = c$, where c is a constant, or equivalently $x = x(s)$, $y = y(s)$ for some parameter s . The tangent vector to the level curves of ψ were calculated from (4.13) with the use of the implicit function theorem. The level curves of ψ were computed by integrating the tangent vector using a Runge–Kutta numerical method starting with the initial conditions

$$x(0) = x_0, \quad y(0) = y_0, \quad (5.4)$$

where (x_0, y_0) is a reference point in the cross section. The same method was used to compute the contours of the axial velocity, i.e. $v_3^* = c$, where c is again a constant.

(d) *Results of the calculations for circular pipes of circular cross section*

Central to the problem of viscous flow in curved pipes is the determination of the friction loss factor f for which, as already indicated in §1*a*, there is an abundance of experimental data and significant recent numerical solutions obtained from the Navier–Stokes equations. In the present analysis of the problem via the direct theory of Part I, the friction loss factor is calculated from (4.18) for circular pipes of circular cross section. These calculations were carried out for several hierarchies corresponding to $H = 5, 6, \dots, 16$. (With reference to the calculations under discussion, the lowest hierarchy to which all of the conditions (2.8)–(2.10) and the incompressibility condition are satisfied is $H = 5$ and the last hierarchy for which calculations were performed is $H = 16$.) The calculations were performed for a non-zero curvature ratio which we took to be $\delta = 0.01$. The results for friction loss are displayed in figures 3–5, where the logarithm of the friction loss factor f is plotted

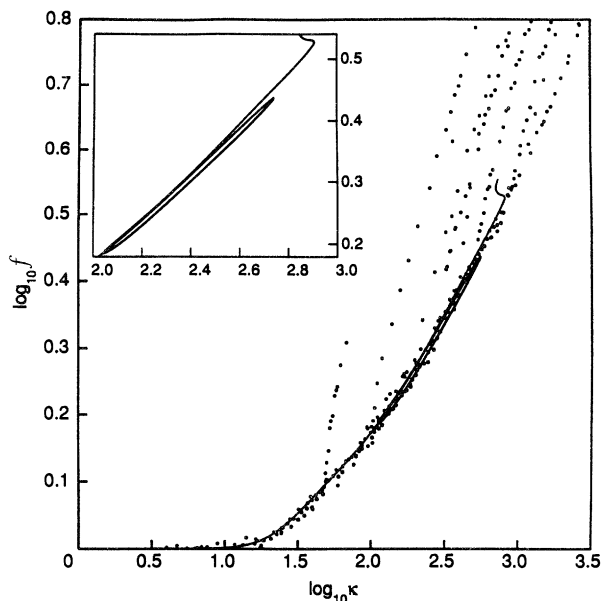


Figure 4. Same caption as that for figure 3, except that the results shown are for the 12th hierarchy.

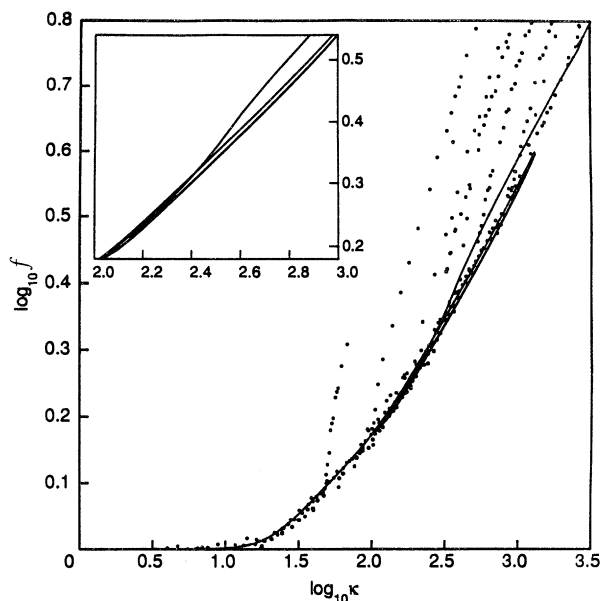


Figure 5. Same caption as that for figure 3, except that the results shown are for the 16th hierarchy.

versus the logarithm of the Dean number κ . This manner of displaying the results for the friction loss is particularly convenient for comparison with experimental results in the literature. Also shown in figures 3–5 is all the experimental data from Itō (1959), exhibited here simply as dots.

At this point in our discussion, it will be helpful to recall that the calculations in *Phil. Trans. R. Soc. Lond. A* (1993)

the recently published numerical solutions (Yang & Keller 1986, among others) were confined to the range up to $\log \kappa \approx 3$. In this connection, it should be noted that the calculations of the present study based on the analytical solution (from the direct theory) for the friction loss, were actually carried to the extent of $\log \kappa \approx 4$ but displayed in figure 5 for the 16th hierarchy only up to $\log \kappa = 3.5$. This result is in very good agreement with both the available experimental data and the numerical solutions that will be discussed presently. Strictly speaking, the inclusion of figure 5 would have sufficed for the purpose of indicating the nature of the agreement just discussed. However, the display of results in figures 3 and 4 from two additional hierarchies lower than $H = 16$ indicates the nature of the improvement in the desired solution with increasing order of hierarchies starting with $H = 8$ in figure 3.

As explained in §5*a*, the calculations of the friction loss were made for a wide range of Dean number, starting from a very small value, less than $\log \kappa = -1$ and increasing in small steps. The calculated friction loss is observed to increase with κ (see figures 3–5) and in the range $-1 < \log \kappa < 0$ is in close agreement for every hierarchy with the linearized solutions (described in §1), which were obtained from the Navier–Stokes equations. For larger values of Dean number, $\log \kappa > 1$, the friction loss curve departs from the linear solution significantly but follows Hasson's envelope of the experimental data. For the eighth hierarchy (see figure 3) the curve leaves the envelope near $\log \kappa \approx 2.5$ (corresponding to $\kappa \approx 320$), and as the hierarchy is increased the departure is postponed until larger values of Dean number. The nature of the range of validity is obvious from the figures 3–5. The lower hierarchies (like $H = 8$ and 9) provide good results in the early range but do not capture all the features like multiplicity of solutions. Such details are brought out for increasing values of H as in figure 4.

In the range of Dean number $2 < \log \kappa < 3$ (or $100 < \kappa < 1000$) the graph of the friction loss has an interesting behaviour with increasing values of H , as can be seen by the inset graphs in figures 3–5. The departure of the friction loss curve from the envelope of data points is alternately below and above the envelope, for the eighth, ninth and tenth hierarchy. The calculations for the tenth hierarchy then exhibit a multiple solution in this range which occurs as a loop in the friction loss curve. Subsequent extensive calculations using the lower hierarchies were unable to reveal this feature. The loop which occurs in the tenth hierarchy remains but becomes narrower as the hierarchy is increased. Beyond the 12th hierarchy the loop does not change except that it lengthens (at larger κ) with increasing hierarchy. Also at the 12th hierarchy (figure 4) a second loop starts to form, is accentuated in the 14th hierarchy but as may be seen from figure 5 does not appear in the 16th hierarchy until $\log \kappa \approx 3.5$.

Four bifurcation (or limit) points were found in the course of calculations from the equations of the 16th hierarchy. Their locations in the plot of the friction loss curve (identified by values on the abscissa and the ordinate) in figure 5 are listed in table 2. By following the friction loss curve of figure 5 from the origin, the limit point corresponding to $\log \kappa = 3.119$ is encountered first; then turning back and following the curve with Dean number decreasing, one encounters the limit point at $\log \kappa = 2.044$. Continuing we cross the limit points at $\log \kappa = 3.457$ and $\log \kappa = 3.398$ in succession.

Recalling figure 2*a* and *b* described in §1*a*, which are converted plots (in terms of $\log f$ against $\log \kappa$) from Yang & Keller (1986, figures 2 and 3), we note once more that these two figures correspond to their numerical solution of the Navier–Stokes

Table 2. *Bifurcation points in figure 5*

Dean number κ	logarithm of κ	friction loss f
1316	3.119	3.978
110.7	2.044	1.525
2861	3.457	5.994
2502	3.398	5.774

Table 3. *A comparison of bifurcation points from several recent studies*

present paper	Dennis & Ng (1982)	Winters & Brindley (1984)	Yang & Keller (1986)	Daskopoulos & Lenhoff (1989)
29610	NA	NA	25 146	32 510
955	956	968	955	956
97 000	NA	NA	15 643	NA
81 720	NA	NA	7 724	2 494

equations with zero curvature ratio ($\delta = 0$) for two different discretization mesh sizes: figure 2*a* represents results using coarser mesh calculations than those of figure 2*b*. From a comparison of figure 5 with the corresponding numerical solution of Yang & Keller for the friction loss factor (in figure 2*a* and *b*), one can easily conclude a very good agreement between the two results. Similarly, very good agreement can be observed with the tabular and graphical results of Dennis (1980), Dennis & Ng (1982), Soh & Berger (1987) and Daskopoulos & Lenhoff (1989).

With reference to the overall variation of the friction loss factor f versus the Dean number κ , in the preceding paragraph we have indicated favourable comparisons between the prediction of the analytical solution of this paper and the corresponding results from several recent numerical solutions of the problem. We now turn to a more detailed comparison of the location of the limit points found in the solution depicted in figure 5 with corresponding results reported in the papers of Dennis & Ng (1980), Winters & Brindley (1984), Yang & Keller (1986) and Daskopoulos & Lenhoff (1989). The comparison sought is best carried out by using an alternative Dean number D defined by

$$D = Re_0(2\delta)^{\frac{1}{2}}, \quad (5.8)$$

since these papers all use the definition of Dean number in (5.8) in their computations and since the corresponding values of the friction loss factor were not reported in all of these papers. A list of the bifurcation (or limit) points from the papers cited, together with the converted version of those in table 2 in terms of D , is given in table 3. The entries in table 3 labelled NA indicate that the corresponding numerical solutions did not exhibit this limit point.

To continue the discussion of the limit points summarized in table 3, again we observe that the first, third and fourth limit points were not found in the early studies of Dennis & Ng (1982) and Winters & Brindley (1984). The more recent numerical solutions of Yang & Keller (1986) and Daskopoulos & Lenhoff (1989) predict that the first limit point occurs for the Dean number D of 25 146 and 32 510, respectively. The second limit point was found by all investigators cited above and corresponds very closely to the value $D = 955$. The third limit point was not found by Yang & Keller (1986) in their calculations using a less refined mesh but was found by them with the more refined mesh to be $D = 15 643$; and, similarly, the fourth limit

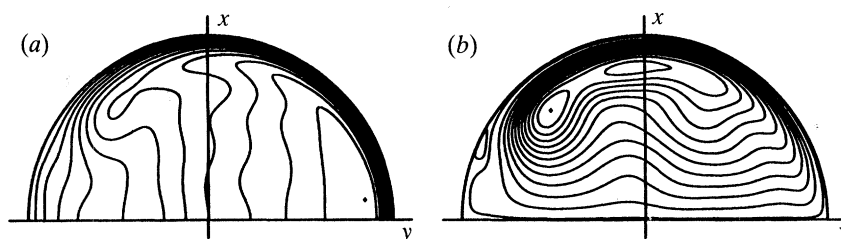


Figure 6. Contours of (a) the axial velocity and (b) the streamlines for the cross-flow as predicted by the direct theory (16th hierarchy, circular cross section, curvature ratio $\delta = 0.01$) for a value of the Dean number $\kappa = 1011.3$ and friction loss $f = 3.5577$ and corresponding to the results shown in figure 5. Only one-half of the cross section is shown due to the symmetry about the y -axis.

point $D = 7724$ was found only with the refined mesh. Daskopoulos & Lenhoff (1989) did not find a limit point corresponding to the third limit point but did find the fourth limit point at $D = 2494$. It should also be noted that the detailed nature of the flow corresponding to solutions on the fourth and fifth branch (related to the entries in the third and fourth row of table 3) is not in good agreement between the various numerical solutions cited above, which perhaps explains the discrepancy between the results for the third and fourth limit points. Another explanation of this discrepancy can be inferred from the calculations of Yang & Keller (1986), who used two discretizations of their governing equations. Since the less refined calculations of Yang & Keller did not reveal the third and fourth limit points while the more refined calculations did, it seems that the predicted numerical value of these limit points is very sensitive to the accuracy of the computations. This observation is also borne out by recalling that the computation is sensitive to numerical round off error especially for large Dean number and that the discrepancies noted above occur primarily when the limit point corresponds to a large Dean number; in fact, the prediction of all investigators agree for the second limit point, which corresponds to a relatively small Dean number. Given the fact that computational errors can be more easily avoided in any analytical solution in contrast to any numerical solution of the same problem, on the basis of results recorded in table 3, one could argue that the analytical solution presented here yields more accurate predictions of the limit points than the purely numerical solutions obtained from the Navier–Stokes equations. Given the fact that both papers of Yang & Keller (1986) and of Daskopoulos & Lenhoff (1989) speculate the possible existence of several branches of the friction loss curve for large Dean number, it may be that their limit points in rows three and four of table 3 do not correspond to the same solution branch. In fact, Daskopoulos & Lenhoff have suggested that their computed solution branch – which gives rise to the values of the limit points in the third and fourth rows of the last column in table 3 – is not the same as that computed by Yang & Keller.

(e) Further remarks on the detailed nature of the flow

It should be evident from the earlier developments that the kinematical ingredients of the direct theory can be interpreted in terms of the velocity \mathbf{v}^* in the three-dimensional theory by adopting a representation of the form (3.4) or (4.11). The representation (4.11) will be used in this section to gain further insight into the predictions of the direct theory with particular reference to the nature of the multiple solutions described in §5*d*.

We recall that for a given value of κ , the system of equations (4.19) and (4.20) determines the non-dimensional director velocities (X_N, B_M) defined by (4.2). Substitution of the solution (X_N, B_M) into (4.11) results in a representation of the three-dimensional velocity field for a given κ . This latter representation and the method of §§5*a–c* are then used to calculate (*a*) level curves of the axial component of the velocity v_3^* from (4.11)₃ and (*b*) level curves (streamlines) of the stream function ψ defined by (4.13). The results of two of these calculations for the 16th hierarchy are shown in parts (*a*) and (*b*), respectively, of each of the figures 6 and 7; the plots in each figure correspond to a given value of the Dean number κ and the curvature ratio $\delta = 0.01$. With reference to figure 1 which shows a diagram of the curved pipe and the rectangular cartesian coordinate system $x = (x_1, x_2, x_3)$ used there, recall from (4.1) the non-dimensional curvilinear coordinates $x = \zeta^1/a$, $y = \zeta^2/b$, which are in the direction of $\mathbf{a}_1, \mathbf{a}_2$, respectively and note that the axis of rotation of the pipe (which coincides with the x_1 -axis) is parallel to the direction of the non-dimensional coordinate x or simply the x -axis. Keeping this in mind and with reference to any one of figures 6 and 7, we observe that the point on the negative y -axis at the left edge of the cross section corresponds to the inner radius of the pipe and that the point on the positive y -axis at the right edge of the cross section corresponds to the outer radius. In the subsequent discussion we frequently refer to these two points in the cross section. A small 'plus-sign' symbol is shown in the cross section of each part (*a*) and (*b*) of figures 6 and 7, which locates the point in the cross section of the maxima of the absolute value of the axial velocity v_3^* and the stream function ψ , respectively. Level curves are drawn in both parts (*a*) and (*b*) of figures 6 and 7 corresponding to integer multiples of the maximum value of each function multiplied by $1/11$. An additional streamline (the one nearest the pipe wall, in all cases, since the stream function vanishes at the wall) corresponding to $1/110$ (i.e. one tenth of the spacing of the other streamlines) of the maximum value of the stream function is also drawn in part (*b*) of each of figures 6 and 7.

Observations made by this procedure regarding the nature of the flow are described below, but the corresponding figures showing the streamlines and axial velocity contours are omitted wherever possible for compactness. The computed contours of the axial velocity and the stream function for relatively small values of Dean number show a cross-flow structure similar to the approximate solutions of Dean (1928) and existing numerical solutions of the Navier–Stokes equations (Daskopoulos & Lenhoff 1989, fig. 1*a*). The flow corresponds to two symmetric counter-rotating vortices, one in each half of the cross section. The maximum value of the axial velocity occurs at a point near the origin and the maximum value of the stream function occurs at a point on the x -axis. As the Dean number is increased, the contours of the axial velocity and the streamlines shift toward the outer radius of the curved pipe. For larger values of κ , the axial velocity contours become concave near the location of the maximum of the axial velocity which is displaced towards the outer radius and the location of the maximum of the stream function moves inward, having reversed its previous trend which was outward. These features have been observed in previous numerical solutions (Collins & Dennis 1975, figs 2*a, b* and 3*a, b*; Daskopoulos & Lenhoff 1989, fig. 1*b*). Further increase in the Dean number is accompanied by accentuation of the concavity of the contours (the streamlines also become concave) which is similar to existing numerical results (Collins & Dennis 1975, figs 2*c, d* and 3*c, d*; Yang & Keller 1986, fig. 4; Soh & Berger 1987, figs 7*a, b*; Daskopoulos & Lenhoff 1989, fig. 1*c*). Just before the first limit point is reached, the

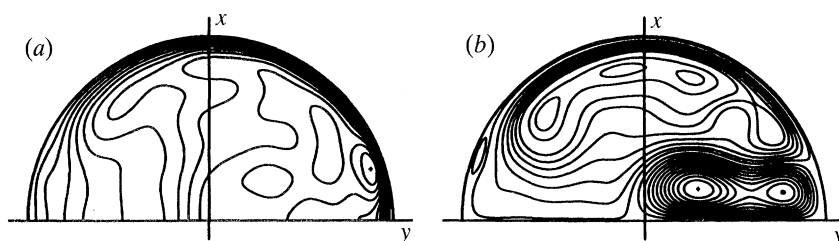


Figure 7. Same caption as that for figure 6, except that the result shown corresponds to cross-flow for a value of the Dean number $\kappa = 1015.5$ and friction loss $f = 3.9036$.

cross-flow exhibits two features as seen in figure 6; the maximum of the axial velocity moves off the y -axis, which is evidence of a doubly peaked axial velocity profile, and the stream function develops both a separate local maximum and a small recirculating region near the inner radius, as can be seen by the two narrowest contours in figure 6*b*. This latter feature has not been reported before, but may be present in the solutions of Soh & Berger (1987, fig. 7*c*) where streamlines show a local perturbation near the inner radius, but they did not plot enough streamlines to bring out this feature. By following the folded friction loss curve with decreasing Dean number along the second branch of the friction loss curve, one finds that the flow is similar to figure 6. A continued decrease in the Dean number along this solution branch precipitates the appearance of a small secondary vortex near the outer radius and disappearance of both the vortex at the inner radius and the local maximum of the stream function. This secondary vortex is similar to previously reported numerical solutions (Daskopoulos & Lenhoff 1989, fig. 5*c*). As the Dean number is further decreased, the vortex enlarges and displaces the axial flow from the y -axis. By traversing the second limit point and increasing the Dean number to follow the third branch of the friction loss curve, we see a 'pinching' of the secondary vortex as it extends radially inward and that the local maxima (or peaks) of the axial velocity become more pronounced while shifting towards the inner radius. These observations are similar to those already reported by Daskopoulos & Lenhoff (1989, fig. 4*b, c*) and Yang & Keller (1986, fig. 6). Further increase in the Dean number along the third branch gives a flow similar to that shown in figure 7. The 'pinching' of the secondary vortex in figure 7*b* gives rise to two local maxima of the stream function in the secondary vortex. Local maxima also appear in the stream function main vortex and a small recirculating region arises at the inner radius. In addition to the absolute maximum of the axial velocity marked by a 'plus sign' in figure 7, the axial velocity contours also exhibit two local maxima not too far from the absolute maximum. There are no published results corresponding to this last figure; however, two different results for nearly the same Dean number have appeared in the literature. The first is by Yang & Keller (1986, fig. 9) which they obtained for a curvature ratio of zero. Their results show a complex cross-flow structure which indicates the presence of six vortices in the cross section. Also, Soh & Berger (1987, fig. 7*c*) display the stream function for a comparable value of Dean number but for a curvature ratio of $\frac{1}{10}$. Their cross-flow streamlines do not exhibit a secondary vortex at all; the cross-flow appears very similar to that of our large Dean number solutions on the first branch.

The work of two of us (P.M.N. and M.J.S.) was supported by the U.S. Office of Naval Research under Contract N00014-86-K-0057, R & T 4322-534 with the University of California at Berkeley.

Phil. Trans. R. Soc. Lond. A (1993)

Appendix A

The purpose of this Appendix is to provide an outline of calculations of the non-dimensional version of the constitutive coefficients which occur in the reduced form of the equations of motion (4.8) and (4.9). Preliminary to this development, we observe that the constitutive equations in the theory (prior to non-dimensionalization) involve a number of integrals of the type

$$\alpha_{kl}^{ij}(\delta) = \frac{1}{2\pi} \iint_A x^i y^j \mu_1^k (1 + \delta y)^l dx dy \quad (\text{A } 1)$$

over the cross section A of the pipe, where each of the superscripts i, j, k, l on the right-hand side of (A 1) indicates power and can assume both odd and even positive integer values.

For an explicit closed form evaluation of the integral in (A 1), it is expedient to map the cross-sectional area onto a unit circle using (4.1)_{1,2} and (4.6) in the x - y plane of integration and then introduce a change of variables in terms of polar coordinates. As a consequence of this transformation, the integrand in (A 1) will involve trigonometric functions and after several integration by parts we obtain

$$\left. \begin{aligned} \alpha_{kl}^{ij}(\delta) &= \sum_{r=0}^l \sum_{s=0}^k \left[\binom{l}{r} \binom{k}{s} \frac{(-1)^s \delta^r}{i+j+r+2(s+1)} \frac{(i-1)!!(j+r-1)!!}{(i+j+r)!!} \right], & \text{for even integer} \\ & & \text{values of } i, j \\ \alpha_{kl}^{ij}(\delta) &= 0, & \text{otherwise.} \end{aligned} \right\} \quad (\text{A } 2)$$

Also, in (A 2) the symbol $\binom{i}{j}$ is the usual binomial coefficient, the double factorial notation $!!$ (Abramowitz & Stegun 1965, p. 258) for positive integers n is defined as

$$(2n)!! = 2.4.6 \dots (2n), \quad (2n-1)!! = 1.3.5 \dots (2n-1), \quad (\text{A } 3)$$

and we have also adopted the convention that $0!! = (-1)!! = 1$.

To illustrate the nature of the process of calculations, consider one of the constitutive coefficients in (4.8)–(4.9), namely

$$F_{NMR} = - \iint_A \lambda_N^2 \lambda_M^3 \lambda_R^3 dx dy, \quad (\text{A } 4)$$

which accompanies the kinematical variables $w_{M3}^3 w_{R3}^3$ as part of one term in the equation of motion (4.9). Before proceeding further, it is worth observing that the coefficient F_{NMR} is symmetric in M and R and this reduces the task of computation of its components from (A 4). Similarly symmetry or skew-symmetry properties can be observed from corresponding integral representations of other coefficients such as A_{NM} , C_{NMR} , D_{NM} and the expression for $(C_{NMR} - \delta F_{MNR})$. These symmetry properties, of course, are also implied by the final form of the expressions after executing the integration but they are less transparent (see, for example, (A 6) below).

Substitution of (4.5) into (A 4) yields

$$F_{NMR} = \iint_A (1 + \delta y) \mu_1^3 x^{i_R + i_M + i_N} y^{j_R + j_M + j_N} (4x^2 - (i_N + 1) \mu_1) dx dy. \quad (\text{A } 5)$$

The latter result can be integrated with the help of (A 1) to give

$$F_{NMR} = 2\pi(4\alpha_{31}^{(I+2)J} - (i_N + 1)\alpha_{41}^{IJ}), \quad (\text{A } 6)$$

where we have also introduced the notations

$$I = i_R + i_M + i_N, \quad J = j_R + j_M + j_N. \quad (\text{A } 7)$$

Other constitutive coefficients in the theory can be evaluated similarly from the following list:

$$A_{NM} = - \iint_A [-\delta^2 \lambda_N^3 \lambda_M^3 / (1 + \delta y) + \delta \lambda_N^3 \lambda_M^3, y - (1 + \delta y) \epsilon^2 \lambda_N^3, x \lambda_M^3, x + \delta \lambda_N^3, y \lambda_M^3 - (1 + \delta y) \lambda_N^3, y \lambda_M^3, y] dx dy, \quad (\text{A } 8)$$

$$C_{NMR} = - \iint_A [\delta \lambda_N^3 \lambda_M^2 \lambda_R^3 + (1 + \delta y) (\epsilon \lambda_N^3 \lambda_M^1 \lambda_R^3, x + \lambda_N^3 \lambda_M^2 \lambda_R^3, y)] dx dy, \quad (\text{A } 9)$$

$$D_{NM} = - \iint_A [2\delta^2 \lambda_N^2 \lambda_M^2 / (1 + \delta y) + (1 + \delta y) (2\epsilon^2 \lambda_N^1, x \lambda_M^1, x + \lambda_N^1, y \lambda_M^1, y + \epsilon \lambda_N^1, y \lambda_M^2, x + \epsilon^2 \lambda_N^2, x \lambda_M^2, x + \epsilon \lambda_N^2, x \lambda_M^1, y + 2\lambda_N^2, y \lambda_M^2, y)] dx dy, \quad (\text{A } 10)$$

$$E_{NMR} = \iint_A (1 + \delta y) [\lambda_N^1 \lambda_M^1, x \lambda_R^1 + \lambda_M^1, y \lambda_R^2 + \lambda_N^2 (\epsilon \lambda_M^2, x \lambda_R^1 + \lambda_M^2, y \lambda_R^2)] dx dy. \quad (\text{A } 11)$$

References

- Abramowitz, M. & Stegun, I. A. (eds) 1965 *Handbook of mathematical functions with formulas, graphs and mathematical tables*. New York: Dover.
- Adler, M. 1934 Strömung in gekrümmten Rohren. *Z. Angew. Math. Mech.* **14**, 257–275.
- Barua, S. N. 1963 On secondary flow in stationary curved pipes. *Q. Jl Mech. appl. Math.* **16**, 61–77.
- Berger, S. A., Talbot, L. & Yao, L.-S. 1983 Flow in curved pipes. *A. Rev. Fluid Mech.* **15**, 461–512.
- Cheng, K. C., Inaba, T. & Akiyama, M. 1983 Flow visualization studies of secondary flow patterns and centrifugal instability in curved circular and semicircular pipes. *Flow visualization III* (ed. W. J. Yang), pp. 531–536. In *Third Int. Symp. on Flow Visualization, 1983*.
- Collins, W. M. & Dennis, S. C. R. 1975 The steady motion of a viscous fluid in a curved tube. *Q. Jl Mech. appl. Math.* **28**, 133–156.
- Daskopoulos, P. & Lenhoff, A. M. 1989 Flow in curved ducts: bifurcation structure for stationary ducts. *J. Fluid Mech.* **203**, 125–148.
- Dean, W. R. 1927 Note on the motion of fluid in a curved pipe. *Phil. Mag.* **4**, 208–223.
- Dean, W. R. 1928 The stream-line motion of fluid in a curved pipe. *Phil. Mag.* **5**, 673–695.
- Dennis, S. C. R. 1980 Calculation of the steady flow through a curved tube using a new finite-difference method. *J. Fluid Mech.* **99**, 449–467.
- Dennis, S. C. R. & Ng, M. 1982 Dual solutions for steady laminar flow through a curved tube. *Q. Jl Mech. appl. Math.* **35**, 305–324.
- Eustice, J. 1910 Flow of water in curved pipes. *Proc. R. Soc. Lond. A* **84**, 107–118.
- Green, A. E. & Naghdi, P. M. 1993 A direct theory of viscous flow in pipes. I. Basic general developments. *Phil. Trans. R. Soc. Lond. A* **342**, 525–542. (Preceding paper.)
- Hasson, D. 1955 Streamline flow resistance in coils. *Res. Corresp.* **8**, S1.
- Itō, H. 1959 Friction factors for turbulent flow in curved pipes. *J. basic Engng* **81**, 123–132.
- Itō, H. 1969 Laminar flow in curved pipes. *Z. Angew. Math. Mech.* **11**, 653–663.
- Itō, H. 1987 Flow in curved pipes. *JSME Int. J.* **30**, 543–552.
- Keulegan, G. H. & Beij, K. H. 1937 Pressure losses for fluid flow in curved pipes. *J. Res. natl Bureau Standards* **18**, 89–114.
- Phil. Trans. R. Soc. Lond. A* (1993)

- Larraiin, J. & Bonilla, C. F. 1970 Theoretical analysis of pressure drop in the laminar flow of fluid in a coiled pipe. *Trans. Soc. Rheology* **14**, 135–147.
- Naghdi, P. M. 1982 Finite deformation of elastic rods and shells. In *Proc. IUTAM Symp. on Finite Elasticity, Bethlehem, PA, 1980* (ed. D. E. Carlson & R. T. Shield), pp. 47–103. The Hague: Martinus Nijhoff.
- Pedley, T. J. 1980 *The fluid mechanics of large blood vessels*. Cambridge University Press.
- Powell, M. J. D. 1970 A hybrid method for nonlinear equations. In *Numerical methods for nonlinear algebraic equations* (ed. P. Rabinowitz), pp. 87–114. New York: Gordon and Breach.
- Ramshankar, R. & Sreenivasan, K. R. 1988 A paradox concerning the extended Stokes series solution for the pressure drop in coiled pipes. *Phys. Fluids* **31**, 1339–1347.
- Soh, W. Y. & Berger, S. A. 1987 Fully developed flow in a curved pipe of arbitrary curvature ratio. *Int. J. numer. Meth. Fluids* **7**, 733–755.
- Taylor, G. I. 1929 The criterion for turbulence in curved pipes. *Proc. R. Soc. Lond. A* **124**, 243–249.
- Topaloglu, H. C. 1967 Steady laminar flows of incompressible fluid in curved pipes. *J. math. Mech.* **16**, 1321–1337.
- Van Dyke, M. 1978 Extended Stokes series: Laminar flow through a loosely coiled pipe. *J. Fluid Mech.* **86**, 129–145.
- Ward-Smith, A. J. 1980 *Internal fluid flow*. Oxford: Clarendon Press.
- White, C. M. 1929 Streamline flow through curved pipes. *Proc. R. Soc. Lond. A* **123**, 645–663.
- Winters, K. H. & Brindley, R. C. G. 1984 Multiple solutions for laminar flow in helically-coiled tubes. U.K. Atomic Energy Authority, Harwell, p. AERE Report 11373.
- Yang, Z. H. & Keller, H. B. 1986 Multiple laminar flows through curved pipes. *Appl. numer. Math.* **2**, 257–271.

Received 21 November 1991; accepted 9 November 1992